　　　　　　　　　　　　　　　　　　　　　　　　　　　　Open Access

Uncovering the mechanisms underlying pear leaf apoplast protein-mediated resistance against *Colletotrichum fructicola* through transcriptome and proteome profiling

Chenyang Han[1], Zhiyuan Su[1], Yancun Zhao[2], Chaohui Li[2], Baodian Guo[2], Qi Wang[1], Fengquan Liu[2*] and Shaoling Zhang[1*]

Abstract

Pear anthracnose, caused by the fungus *Colletotrichum fructicola*, is a devastating disease for the pear industry. The apoplast, an extracellular compartment outside the plasma membrane, plays a crucial role in water and nutrient transport, as well as plant-microbe interactions. This study aimed to uncover the molecular mechanism of pear leaf apoplastic protein-mediated resistance to *C. fructicola*. Apoplast fluid was isolated using the vacuum infiltration method, and defence-related apoplastic proteins were identified through protein mass spectrometry and transcriptome sequencing. We found 213 apoplastic proteins in the leaf apoplast fluid during early *C. fructicola* infection, with the majority (74.64%) being enzymes, including glycosidases, proteases, and oxidoreductases. Gene Ontology analysis revealed their involvement in defence response, enzyme inhibition, carbohydrate metabolism, and phenylpropanoid biosynthesis. Transcriptome analysis showed the infection induced expression of certain apoplast proteins, potentially contributing to pear leaf resistance. Notably, the expression of *PbrGlu1*, an endo-β-1,3-glucanase from the glycoside hydrolase 17 family, was significantly higher in infected leaves. Silencing of the *PbrGlu1* gene increased pear leaf susceptibility to *C. fructicola*, leading to more severe symptoms and higher reactive oxygen species content. Overall, our study provides insights into the apoplast space interaction between pear leaves and *C. fructicola*, identifies a key gene in infected pears, and offers a foundation and new strategy for understanding the molecular mechanisms underlying pear anthracnose and breeding disease-resistant pears.

Keywords *Colletotrichum fructicola*, Pear, Apoplast, Glycoside hydrolases, Plant immunity

*Correspondence:
Fengquan Liu
fqliu20011@sina.com
Shaoling Zhang
slzhang@njau.edu.cn
[1] Center of Pear Engineering Technology Research, State Key Laboratory of Crop Genetics and Germplasm Enhancement, College of Horticulture, Nanjing Agricultural University, Nanjing 210095, China
[2] Institute of Plant Protection, Jiangsu Academy of Agricultural Sciences, Jiangsu Key Laboratory for Food Quality and Safety, State Key Laboratory Cultivation Base of Ministry of Science and Technology, Nanjing 210014, China

Background

Pear, a widely cultivated fruit tree species, is highly susceptible to a diverse range of pests and diseases that can significantly impact crop yield and quality. Among the most devastating diseases impacting the pear industry is pear anthracnose, which is caused by the fungus *Colletotrichum fructicola* (Li et al. 2013; Fu et al. 2019). It is considered as one of the most serious diseases in the major pear-producing regions of China (Fu et al. 2019). It can occur during the growth of pear trees and the ripening of fruits, causing fruit decay and premature leaf loss,

leading to weaken tree vigour (Jiang et al. 2014; Cao et al. 2022). It seriously affects the yield and quality of pears, resulting in significant economic losses.

The plant apoplast is a complex system of intercellular spaces, cell walls, and extracellular fluids that plays a critical role in the transport of water, nutrients, and signalling molecules throughout the plant (Sattelmacher 2000). At the same time, it is also the main battlefield for plant-microorganism interactions (Naseem et al. 2017; Wang et al. 2020). The plant apoplast is defined as the extracellular space external to the plasma membrane, including the cell wall, middle lamella, and intercellular spaces (Sattelmacher 2000). The apoplast is formed by the deposition of cellulose and other polysaccharides by the cell wall, which creates a network of interconnected channels and pores (Dora et al. 2022). This network allows for the diffusion and flow of water and solutes, enabling the exchange of nutrients and signalling molecules between cells (Dora et al. 2022). In studies of host-pathogen interactions, the definition of the apoplast varies due to the differences in the lifestyles of different pathogens. During plant-bacteria interactions, pathogenic bacteria, upon successful invasion of the host through stomata or wounds, colonize the intercellular fluid, undergo multiplication, and establish residence. Throughout this process, the term "apoplast" refers to the region outside the cell membrane, including the plant cell wall and the intercellular fluid (Bai et al. 2015). However, in the case of interactions between plants and biotrophic or hemibiotrophic fungi and oomycetes, the definition of the apoplast different. Pathogens form appressoria on the surface of the plant, which further develop into extra-invasive hyphae, allowing the pathogen to grow and reproduce within the plant while extracting nutrients from plant cells. The extra-invasive hyphae or haustoria are enclosed by specialized membranes derived from the host, known as the extra-invasive hyphal membrane (EIHM) (Kankanala et al. 2007) or extra-haustorial membrane (EHM) (Kwaaitaal et al. 2017). During the arbuscular mycorrhizal (AM) symbiotic process, arbuscular mycorrhizal fungi differentiate highly branched hyphae, each surrounded by a periarbuscular membrane (PAM) derived from the plant (Ivanov et al. 2019). In these processes, the space between the microbial membrane and the plant plasma membrane is defined as the apoplast (Wang et al. 2020).

Hydrolases, including glucosidases, proteases, and lipases, are essential component of the apoplast fluid in plants (Lopez-Casado et al. 2008; Wang et al. 2020; Sueldo et al. 2023). They contribute to various processes, including cell wall remodelling, lignification, and defence against pathogens (Sueldo et al. 2023). A significant portion of the pathogenesis-related (PR) proteins discovered

thus far have been classified as apoplastic hydrolases (Van Loon et al. 2006). These proteins are triggered in plants when attacked by oomycetes, fungi, bacteria, viruses, or insects, with the apoplast being recognized as the primary site for the accumulation of PRs (Zribi et al. 2021). The fungal cell wall is primarily composed of cellulose and chitin, with chitin playing a crucial role in enhancing the strength and stability of the cell wall (Lee et al. 2021). Consequently, when plants face fungal infections, they actively secrete a significant quantity of cell wall-degrading hydrolases to specifically target fungal cell walls (Zribi et al. 2021). Among these hydrolases, chitinases (such as PR-3, 8, and 11) have been extensively studied, and these hydrolases break down chitin polymers by cleaving the β-1,4-glycosidic bonds of chitin molecules using two conserved glutamic acid residues (Gomez et al. 2002; Hong et al. 2002). At the same time, the fungal colonization process involves the secretion of numerous effector molecules, which play a role in suppressing plant defence responses, modifying plant physiology, and facilitating nutrient acquisition by fungi (Giraldo and Valent 2013; Lo Presti et al. 2015). In response, a significant number of plant-derived proteases accumulate in the extracellular region, where they enhance the host's resistance against different types of pathogens (Wang et al. 2019, 2020). Proteases (also known as peptidases) are proteins that catalyse the degradation of other proteins based on their ability to recognize and cleave specific short amino acid sequences (Maxwell 2022). It has been reported that proteases, such as aspartic proteases and serine proteases, are highly enriched in the extracellular region (Qin et al. 2003; Ma et al. 2017; Wang et al. 2021). These proteases contribute to improve host resistance by degrading or inhibiting fungal effectors (Wang et al. 2020).

Currently, research on plant apoplasts primarily relies on the extraction of plant apoplast fluid. To obtain apoplast fluid samples, researchers commonly employ different techniques among which centrifugation method is frequently used (Lohaus et al. 2001; Witzel et al. 2011). The latest method involves centrifuging plant tissues (usually leaves) at specific speed and duration to separate the liquid portion outside of the cell wall and plasma membrane (Gentzel et al. 2019). In this study, we utilized the infiltration-centrifugation method to effectively extract the apoplast fluid from pear leaves in the early stages of *C. fructicola* infection. Through proteomic analysis, we conducted a thorough characterization of the protein composition in the apoplast fluid. Moreover, a transcriptomic analysis facilitated the identification of specific proteins that displayed differential abundance or were specifically induced in response to the presence of the pathogen. This research will enhance the knowledge of the interactions of pear and *C. fructicola* in apoplast.

Results

Experimental design and transcriptome analysis

To elucidate the molecular network of pear leaf apoplastic protein-mediated resistance after inoculation with *C. fructicola*, inoculated leaves and mock-inoculated leaves were sampled at 12, 24, and 48 h post-inoculation (hpi), respectively (Fig. 1a). Of these samples, 12 hpi samples were used for collecting apoplast fluid (Fig. 1b). The analysis of the *C. fructicola* infection based on transcriptome results are shown in Additional file 1: Table S1. An average of 54,671,100 clean reads from 18 samples were obtained, with a Q20 quality score ≥ 96.70%. Moreover, the guanine-cytosine (GC) content in the obtained reads ranged from 46.65 to 49.81%. The filtered reads were aligned with the pear genome (*Pyrus bretschneideri*), and the average mapping percentage reached 73.91%. The correlation between any two of the three replicates for each treatment was > 90% (Fig. 2a).

Identification of differentially expressed genes in *C. fructicola* inoculation and mock inoculation

Compared with the mock-inoculated leaves, a total of 6057 differentially expressed genes (DEGs) at 12 hpi, 6585 DEGs at 24 hpi, and 7210 DEGs at 48 hpi were detected in *C. fructicola*-infected leaves. Among them, 2849, 2721, and 3220 DEGs were downregulated, and 3208, 3864, and 3990 DEGs were upregulated at 12 hpi, 24 hpi, and 48 hpi, respectively. Further comparison of the DEGs revealed that 20.67% downregulated DEGs and 24.99% downregulated DEGs were common to samples at different time points (Fig. 2b, c).

Functional annotation and classification

To comprehend the functions of DEGs in response to *C. fructicola* infection, Gene Ontology (GO) analysis of these genes was performed. A total of 35 GO functions, including those related to 15 molecular functions, 9 cell components, and 11 biological processes, were used to display the differences in samples at different time points (Fig. 2d). Some GO items showed significant differences between downregulated and upregulated DEGs, such as in kinase activity, immune response, and intrinsic component of membrane. In summary, several GO terms related to defence, such as defence response to fungus, immune response, response to chitin, and response to salicylic acid, were significantly enriched in upregulated DEGs. This indicates that pathogenesis-related genes in pear are induced during the early stages of infection.

Identification of apoplast proteins in pear leaves

The apoplast fluid collected from *C. fructicola*-infected leaves was then digested with trypsin and analysed by liquid chromatography-mass spectrometry (LC-MS). In total, 414 proteins were derived from apoplast fluid. The computational prediction of signal peptide cleavage indicated that 51.44% (213) of the proteins possessed a predicted signal peptide (Fig. 3a). In contrast, within the complete proteome of pear, this proportion was significantly lower, standing at only 9.39%. Proteins that are secreted through the general secretory pathway necessitate the presence of a signal peptide (Wei et al. 2021). Consequently, in the subsequent analyses, we refer to proteins containing a signal peptide as apoplastic proteins. The lengths of these proteins are predominantly concentrated at approximately 200–600 aa (Fig. 3b). To comprehend the functions of apoplastic proteins, a GO analysis of these genes was performed. The top ten GO-enriched terms for molecular functions, cell components, and biological processes are shown (Fig. 3c). For cell components, numerous genes were associated with cell walls, vacuoles, and extracellar regions, which are important components of apoplasts. The remarkable enrichment of hydrolase activity and oxidoreductase activity in the molecular function of apoplastic proteins
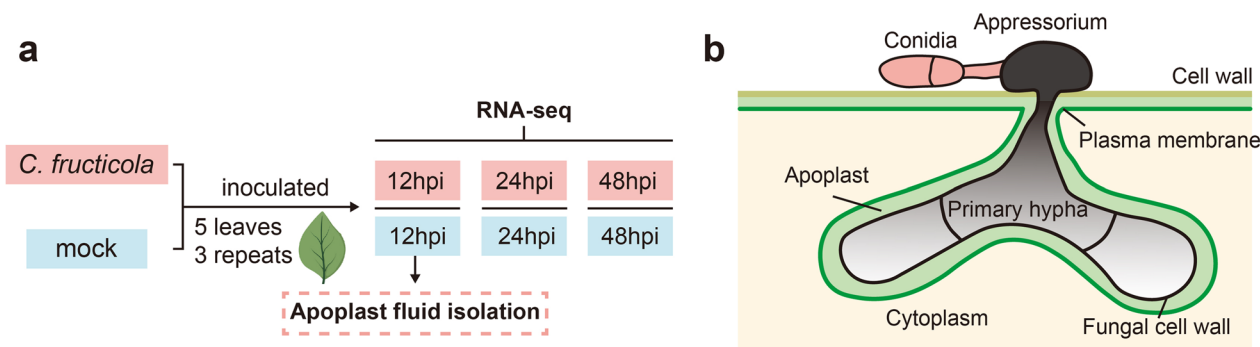

Fig. 1 Detailed drawing of the experimental design. **a** Schematic diagram of sampling for RNA-seq and apoplast fluid isolation. **b** Illustration of the apoplast in a hemibiotrophic process during pear leaf infected by *C. fructicola*
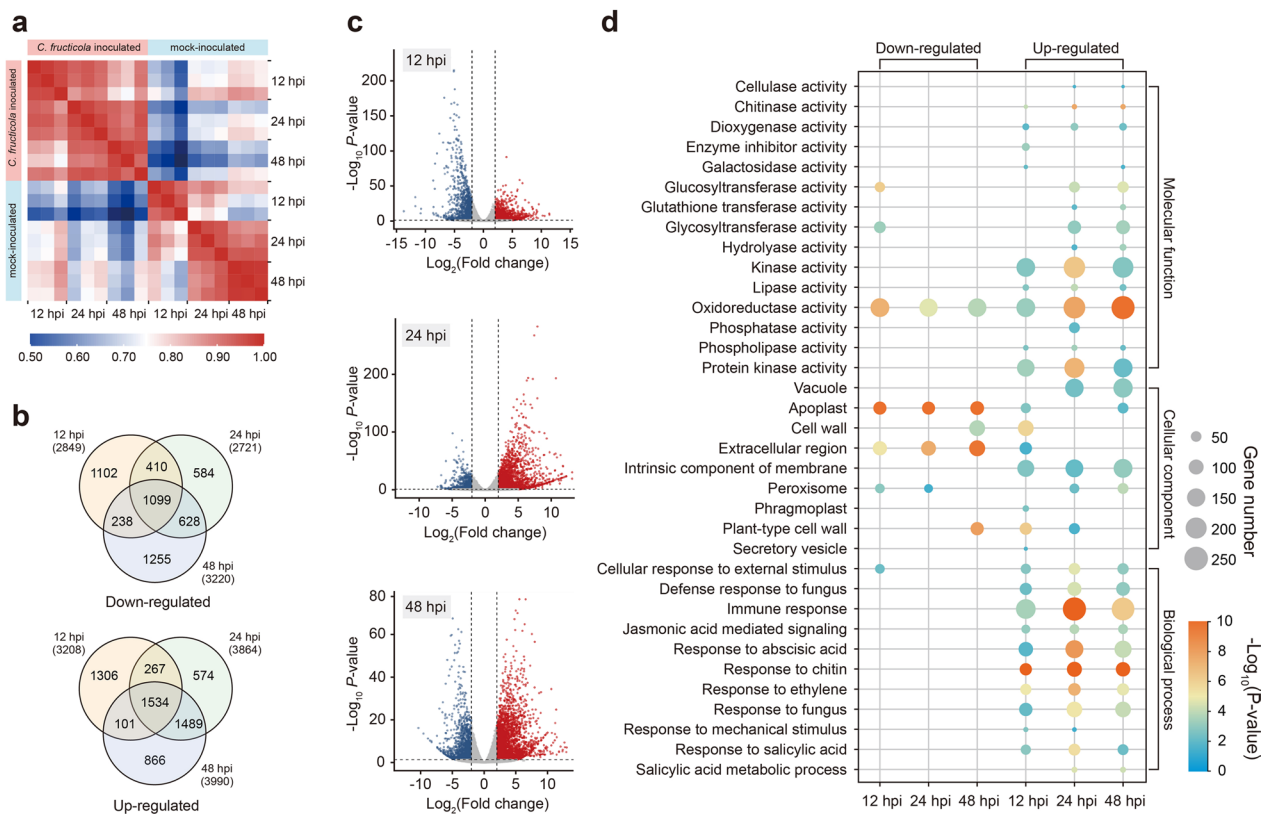
Fig. 2 The responses of pear leaves to *C. fructicola* infection at different time points at the transcriptomic level. **a** Correlation between RNA-Seq samples. **b** Venn diagram showing the number of specific and common upregulated and downregulated DEGs between 12 hpi, 24 hpi, and 48 hpi, respectively. **c** Volcano plot of DEGs between *C. fructicola*-inoculated and mock-inoculated at different time points. **d** GO enrichment analysis of DEGs at various time points during *C. fructicola* infection in key terms

indicate their significant role in potential disease resistance mechanisms. Moreover, the pathway-based analysis of apoplastic proteins mapped nine pathways, including those of phenylpropanoid biosynthesis, carbohydrate metabolism, amino sugar and nucleotide sugar metabolism, biosynthesis of other secondary metabolites, other glycan degradation, peptidases and inhibitors, and other pathways (Fig. 3d). Notably, phenylpropanoid biosynthesis predominantly takes place within the cytoplasm. This finding suggested the diverse functional roles of these proteins, implying that they may have different functions in the cytoplasm and apoplast (Yoshida et al. 2003; Kidwai et al. 2020).

The apoplast fluid contains a high proportion of hydrolases
Classification of these 213 apoplastic proteins using the National Center for Biotechnology Information (NCBI) conserved domain database (CDD, http://www.ncbi. nlm.nih.gov/Structure/cdd/cdd.shtml) and Pfam (http:// pfam.janelia.org) revealed that 53.52% of these apoplastic proteins are hydrolases (Fig. 4 and Additional file 1: Table S2). Oxidoreductases were also important

components of apoplastic proteins, accounting for 13.14%. The other 112 apoplastic proteins were diverse, including auxin-binding protein, epidermis-specific secreted glycoprotein, and lipid-transfer protein, and others.

The 105 detected hydrolases including 71 glycosidases, 26 proteases, and 17 esterases (Fig. 4). As the most abundant class of hydrolases in apoplast, glycosidases comprise 20 different glycosyl hydrolase (GH) families, which include 13 GH17 glycosidases, seven GH18 glycosidases, seven GH64 glycosidases, six GH19 glycosidases, five GH1 glycosidases, five GH28 glycosidases, and 28 other types of glycoside hydrolases (Fig. 4). The detected apoplastic proteases belonged to the mechanistic class of aspartyl proteases (APs, six proteins), serine proteases (SEPs, 11 proteins), cysteine proteases (CPs, six proteins), and other proteases. The 11 SEPs included four subtilisin-like proteases and seven serine carboxypeptidase-like proteases. The six CPs included three papain-like proteases and three caspase-like proteases. The six Asp proteases were all pepsin-like proteases. Finally, the 17 esterases belonged to the mechanistic
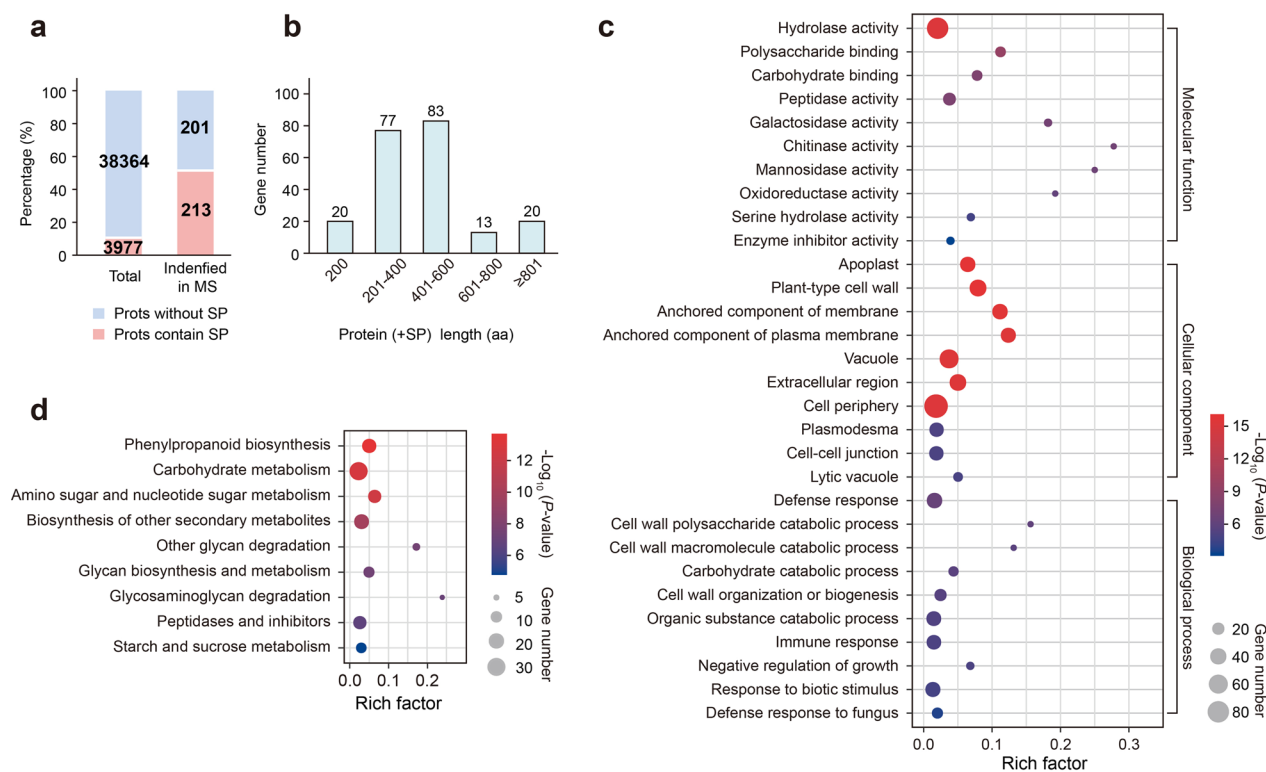
Fig. 3 Functional analysis of apoplastic proteins in pear leaves during *C. fructicola* infection. **a** The proportion of SP-containing proteins in the apoplastic proteins and the total proteome of pear. **b** The distribution of protein lengths in the apoplastic proteins. **c** GO enrichment analysis of apoplastic proteins. **d** KEGG enrichment analysis of apoplastic proteins

class of carboxylic-ester hydrolases, phosphoric-diester hydrolases (PDHs), and phosphoric-monoester hydrolases. The ten carboxylic-ester hydrolases (CEHs) including four pectin acetylesterases, three rectine sterases, and three SGNH hydrolases. This proteome composition exhibited similarities to previously documented proteome in *Arabidopsis thaliana* (Buscaill et al. 2019) and *Nicotiana benthamiana* (Sueldo et al. 2023).

Expression changes of apoplastic hydrolases after *C. fructicola* inoculation

The expression levels of leaf apoplastic hydrolases after *C. fructicola* inoculation were analysed by combining transcriptome data. The scatter plots reveal that the majority of differentially expressed genes exhibit an upregulation trend in response to *C. fructicola* inoculation (Fig. 5a). This is in line with the widely recognized pattern of the accumulation of PR protein, including chitinases and glucanases (Van Loon et al. 2006). Additionally, a substantial induction of oxidoreductases and other proteins occurred following infection. Compared to mock-inoculated leaves, the expression level of some hydrolases in the apoplast increased tenfold upon infection (Fig. 5b, c). Notably, certain glycosidases

belonging to the GH1, GH64, GH17, and GH19 families maintained consistently high expression levels throughout the entire infection process. Across all time points, there were 16 glycosidases whose expression levels were significantly upregulated compared to the mock ($\log_2$FC > 1 and adjusted *P*-value < 0.05), while the expression levels of proteases and esterases did not exhibit such pronounced changes throughout the infection process, with only two proteases and two esterases being significantly upregulated at all time points. Of the two proteases, one is a basic secretory protein (BSP) known as a peptidase of plants and bacteria (*Pbr041409.1*). The particular type of the protease is considered as a component of plant defence mechanisms against pathogens and is categorized within the PR-17 family (Christensen et al. 2002). The other protease belongs to the pepsin family (*Pbr004782.1*), and its counterparts in *Arabidopsis*, *SAP1* and *SAP2*, have been demonstrated to cleave the highly conserved bacterial protein MucD, consequently impeding the growth of *Pseudomonas syringae* (Wang et al. 2019). The two esterases (Pbr033046.1 and Pbr006683.2) are identified as purple acid phosphatase and pectinacetylesterase, respectively, and have also been reported to

a

213 Apoplastic Protein (+SP)

- 71 Glycosidases
- 26 Proteases
- 17 Esterases
- 28 Oxidoreductases
- 70 Other proteins

b

Glycosidase		
Target		**Count**
GH17	Glucan endo-1,3-β-glucosidase	13
GH18	Chitinase	7
GH64	β-1,3-glucanase	7
GH19	Chitinase	6
GH1	β-glucosidase	5
GH28	Polygalacturonase	5
GH5	Endo-β-1,4-glucanase	4
GH16	Xyloglucan	3
GH38	α-mannosidase	3
GH43	β-xylosidase	3
GH127	β-L-arabinofuranosidase	2
GH20	β-hexosaminidase	2
GH31	α-glucosidase	2
GH35	β-galactosidase	2
GH36	α-galactosidase	2
GH79	β-glucuronidase	2
GH27	α-galactosidase	1
GH29	α-L-fucosidase	1
GH45	Endoglucanase	1
GH89	α-N-acetylglucosaminidase	1

Protease	
Target	**Count**
Aspartyl protease	
Pepsin	6
Serine protease	
Serine carboxypeptidase	7
Subtilase	4
Cysteine protease	
Papain	3
Caspase	3

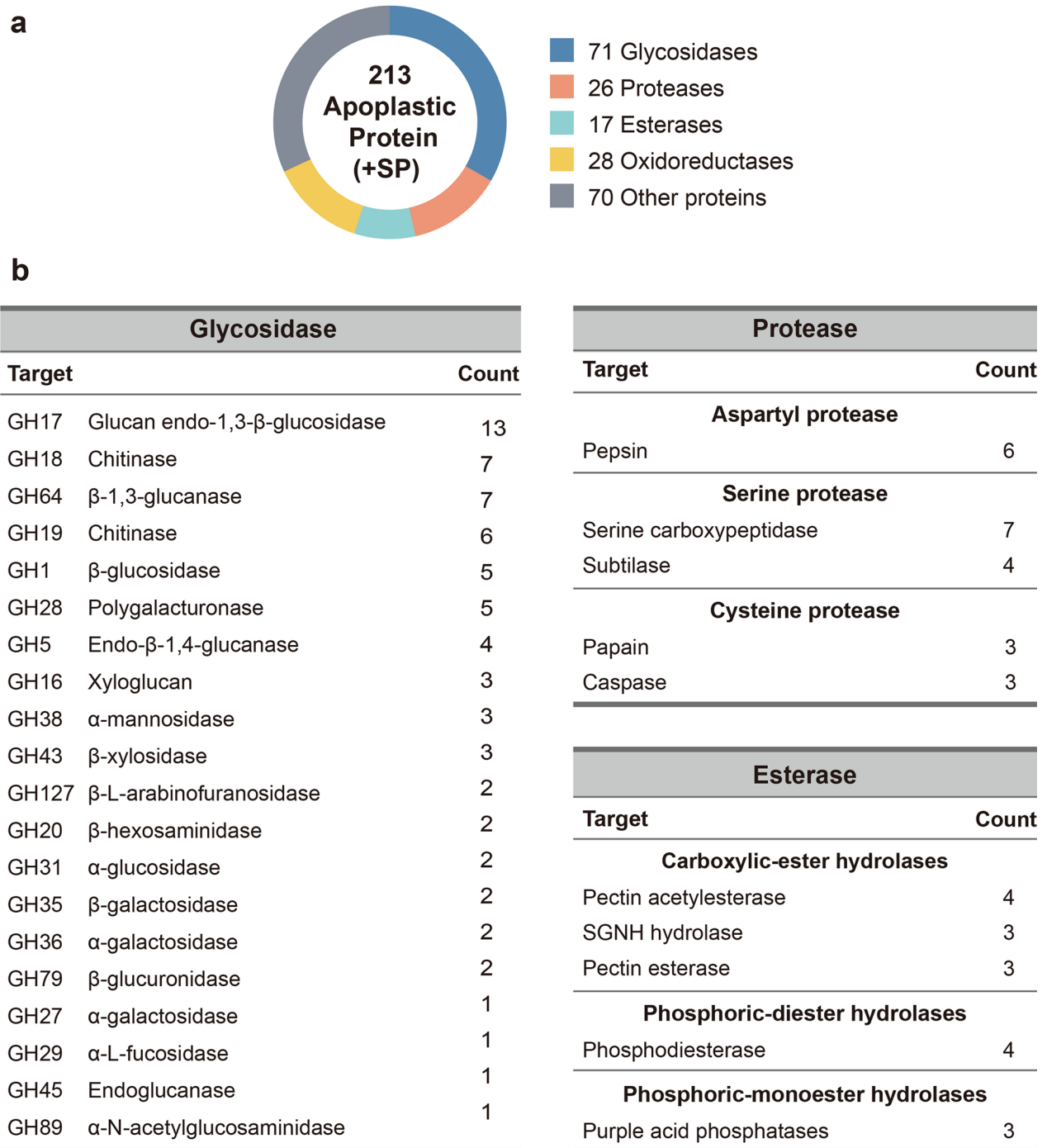| Esterase	
Target	**Count**
Carboxylic-ester hydrolases	
Pectin acetylesterase	4
SGNH hydrolase	3
Pectin esterase	3
Phosphoric-diester hydrolases	
Phosphodiesterase	4
Phosphoric-monoester hydrolases	
Purple acid phosphatases	3

Fig. 4 Composition of apoplast proteins in pear leaves during *C. fructicola* infection. **a** The number of glycosidases, proteases, esterases, oxidoreductases, and other proteins within SP-containing apoplastic proteins. **b** Apoplastic hydrolases were subdivided into protein families

respond to plant environmental conditions (Philippe et al. 2017; Bhadouria and Giri 2022). A subset of genes was selected for quantitative real-time PCR (qRT-PCR) validation (Additonal file 2: Figure S1).

However, in the later stages of infection (48 hpi), there was a notable increase in the number of down-regulated genes. The number of downregulated genes belonging to the glycosidase family increased
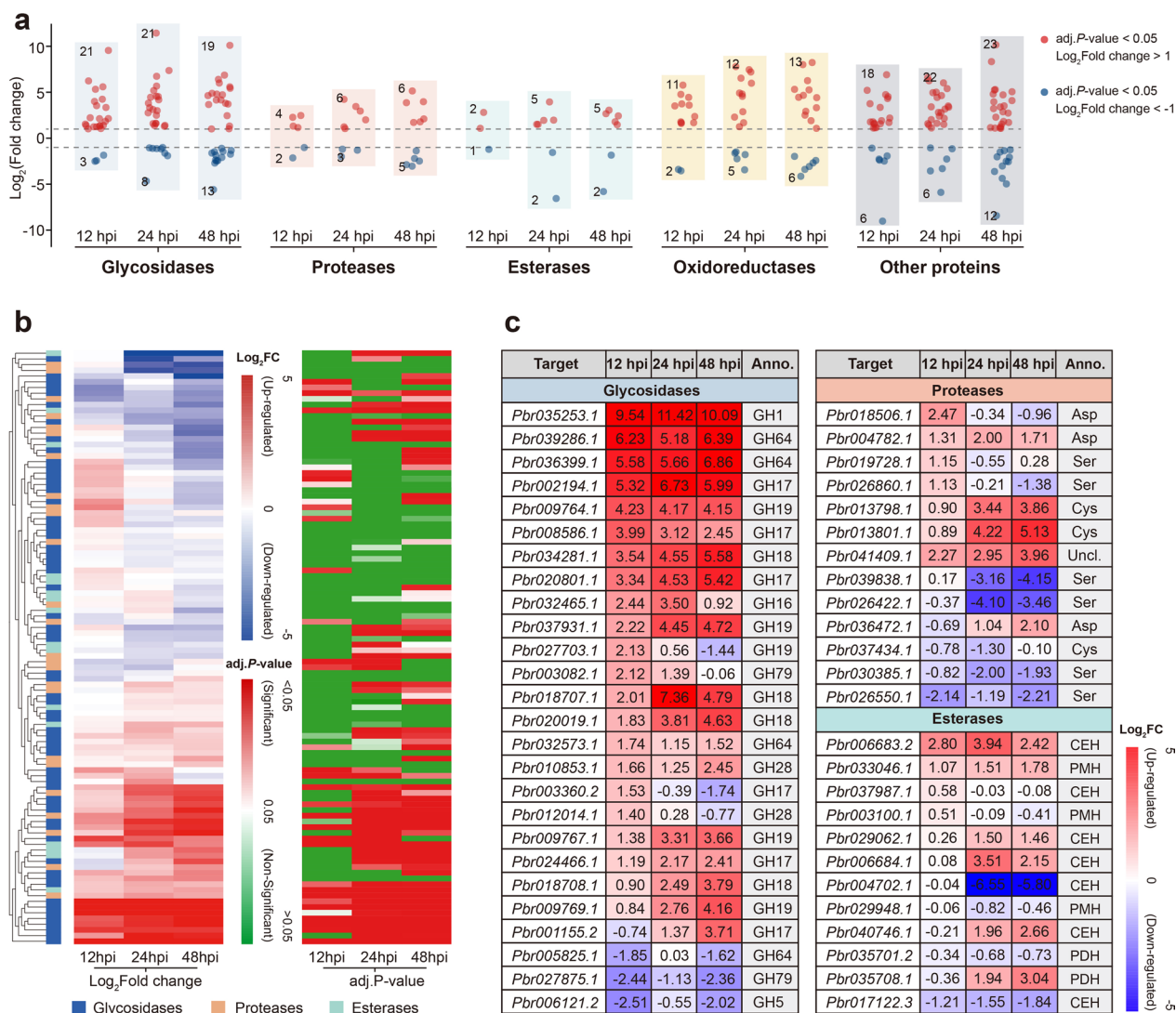
Han *et al. Phytopathology Research* (2024) 6:3

Page 7 of 16

Fig. 5 Expression patterns of apoplastic proteins during *C. fructicola* infection. **a** Expression patterns of significantly differentially expressed apoplastic proteins at 12 hpi, 24 hpi, and 48 hpi. According to their functions, they were classified into five categories: glycosidases, proteases, esterases, oxidoreductases, and other proteins. **b** The heatmap illustrates the expression patterns of all apoplastic hydrolases after *C. fructicola*-inoculation. Red (positive log$_2$-transformed fold change) represents significantly upregulated genes, while blue (negative log$_2$-transformed fold change) represents significantly downregulated genes. The gradient of green color indicates the significance of the adjusted *P*-value (adj.pval). When the adjusted *P*-value is less than 0.05, it is considered to be statistically significant. **c** Annotation and data presentation of representative genes

Part c tables:

Target	12 hpi	24 hpi	48 hpi	Anno.
Glycosidases				
Pbr035253.1	9.54	11.42	10.09	GH1
Pbr039286.1	6.23	5.18	6.39	GH64
Pbr036399.1	5.58	5.66	6.86	GH64
Pbr002194.1	5.32	6.73	5.99	GH17
Pbr009764.1	4.23	4.17	4.15	GH19
Pbr008586.1	3.99	3.12	2.45	GH17
Pbr034281.1	3.54	4.55	5.58	GH18
Pbr020801.1	3.34	4.53	5.42	GH17
Pbr032465.1	2.44	3.50	0.92	GH16
Pbr037931.1	2.22	4.45	4.72	GH19
Pbr027703.1	2.13	0.56	-1.44	GH19
Pbr003082.1	2.12	1.39	-0.06	GH79
Pbr018707.1	2.01	7.36	4.79	GH18
Pbr020019.1	1.83	3.81	4.63	GH18
Pbr032573.1	1.74	1.15	1.52	GH64
Pbr010853.1	1.66	1.25	2.45	GH28
Pbr003360.2	1.53	-0.39	-1.74	GH17
Pbr012014.1	1.40	0.28	-0.77	GH28
Pbr009767.1	1.38	3.31	3.66	GH19
Pbr024466.1	1.19	2.17	2.41	GH17
Pbr018708.1	0.90	2.49	3.79	GH18
Pbr009769.1	0.84	2.76	4.16	GH19
Pbr001155.2	-0.74	1.37	3.71	GH17
Pbr005825.1	-1.85	0.03	-1.62	GH64
Pbr027875.1	-2.44	-1.13	-2.36	GH79
Pbr006121.2	-2.51	-0.55	-2.02	GH5

Target	12 hpi	24 hpi	48 hpi	Anno.
Proteases				
Pbr018506.1	2.47	-0.34	-0.96	Asp
Pbr004782.1	1.31	2.00	1.71	Asp
Pbr019728.1	1.15	-0.55	0.28	Ser
Pbr026860.1	1.13	-0.21	-1.38	Ser
Pbr013798.1	0.90	3.44	3.86	Cys
Pbr013801.1	0.89	4.22	5.13	Cys
Pbr041409.1	2.27	2.95	3.96	Uncl.
Pbr039838.1	0.17	-3.16	-4.15	Ser
Pbr026422.1	-0.37	-4.10	-3.46	Ser
Pbr036472.1	-0.69	1.04	2.10	Asp
Pbr037434.1	-0.78	-1.30	-0.10	Cys
Pbr030385.1	-0.82	-2.00	-1.93	Ser
Pbr026550.1	-2.14	-1.19	-2.21	Ser
Esterases				
Pbr006683.2	2.80	3.94	2.42	CEH
Pbr033046.1	1.07	1.51	1.78	PMH
Pbr037987.1	0.58	-0.03	-0.08	CEH
Pbr003100.1	0.51	-0.09	-0.41	PMH
Pbr029062.1	0.26	1.50	1.46	CEH
Pbr006684.1	0.08	3.51	2.15	CEH
Pbr004702.1	-0.04	-6.55	-5.80	CEH
Pbr029948.1	-0.06	-0.82	-0.46	PMH
Pbr040746.1	-0.21	1.96	2.66	CEH
Pbr035701.2	-0.34	-0.68	-0.73	PDH
Pbr035708.1	-0.36	1.94	3.04	PDH
Pbr017122.3	-1.21	-1.55	-1.84	CEH

from three in the early stage of infection (12 hpi) to 13 in the later stage (48 hpi). It is worth noting that hydrolases belonging to the same family may exhibit different expression patterns during the disease resistance process; for example, certain glycosidases belonging to the GH17, GH19, and GH28 families exhibit upregulation in the early stages of infection, followed by downregulation in the later stages.

Coexpression network of apoplastic hydrolases

During the transcriptome analysis, a substantial number of genes were found to display similar expression patterns. This observation highlights potential coordinated regulation or functional relationships among these genes. To further investigate the interplay between these apoplastic hydrolases, we performed a comprehensive coexpression network analysis utilizing transcriptome data from all 18 samples. In this study, we focused solely on gene pairs that exhibited positive

correlations. After performing Pearson's correlations, 1248 gene pairs consisting of 87 genes with correlation coefficients higher than 0.8 were counted (Fig. 6). Based on their hydrolytic functions, we divided the genes into three main gene clusters. By determining the number of related connections with other genes, we were able to assess the relative importance and influence of each gene within the coexpression network. The various types of hydrolases exhibited a high number of connections, and it is possible that they are regulated by the same or similar transcription factors.

Upon further analysis, we observed that some proteases, such as *Pbr041409.1* (basic secretory proteins), were coexpressed with multiple glycosidase genes, including *Pbr039286.1* (GH64), *Pbr009769.1* (GH19), *Pbr020019.1* (GH18), and *Pbr020801.1* (GH17), suggesting their central roles in coordinating the expression and function of multiple genes within their respective clusters. These highly connected genes may be hub genes that serve as potential key regulators or critical players in the overall functioning of the apoplastic hydrolase network.

Identification and characteristics of the GH17 family in pear

The GH17 family stands out prominently as the most prevalent cluster of glycoside hydrolases discovered within pear leaves. Notably, this family encompasses

certain constituents of the plant PR-2 family (Zribi et al. 2021). Subsequently, we proceeded to ascertain the GH17 constituents within the genome of Chinese white pear (*Pyrus bretschneideri* Rehd. cv. Dangshansuli) utilizing the hidden Markov model search (HMMsearch) technique, employing the GH17 domain HMM profile (PF00332). A total of 68 candidate GH17 genes were identified, and 49 genes were found to have signal peptide-encoding sequences (Additional file 1: Table S3 and Additional file 2: Figure S2). The absence of signal peptides in some GH17 family members may suggest that they are not targeted for secretion or membrane localization. Sixty-one GH17 gene members were mapped onto 16 chromosomes (excluding chromosome 13), and the other seven GH17 genes were located on scaffold contigs (Fig. 7a). Chromosome 2 exhibited the highest count of GH17 genes (20), followed by chromosome 15 with nine genes. The GH17 genes were clustered in fragments of the chromosome instead of being evenly distributed throughout the chromosome. This may be due to uneven duplication events of pear chromosome fragments (Wu et al. 2013).

GH17-a potential source of defence-related apoplastic proteins against pear anthracnose

Combining the transcriptome data, we discovered 47 GH17 genes that were expressed in the leaves, and three gene clusters were identified and visualized in a
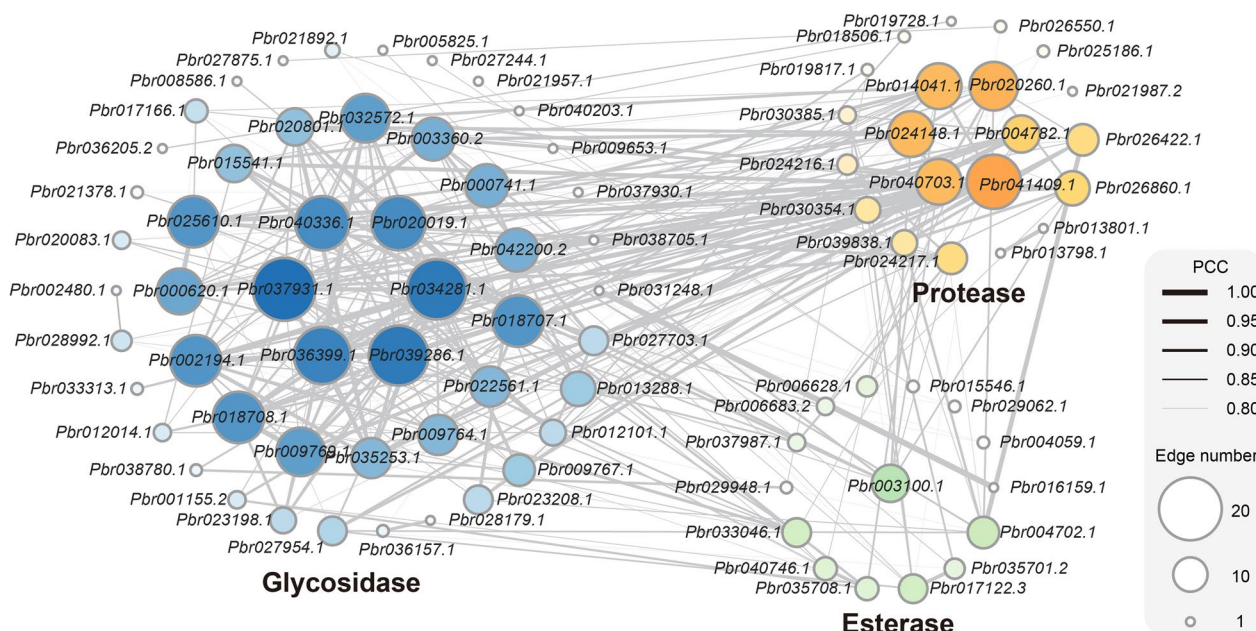

Fig. 6 Co-expression network of apoplastic hydrolases. The size of the circles represents the number of connections each gene has with other genes. The thicker the lines, the higher the correlation coefficient between the genes. The correlation coefficient between pairs of genes was measured using Pearson's correlation coefficient (PCC)
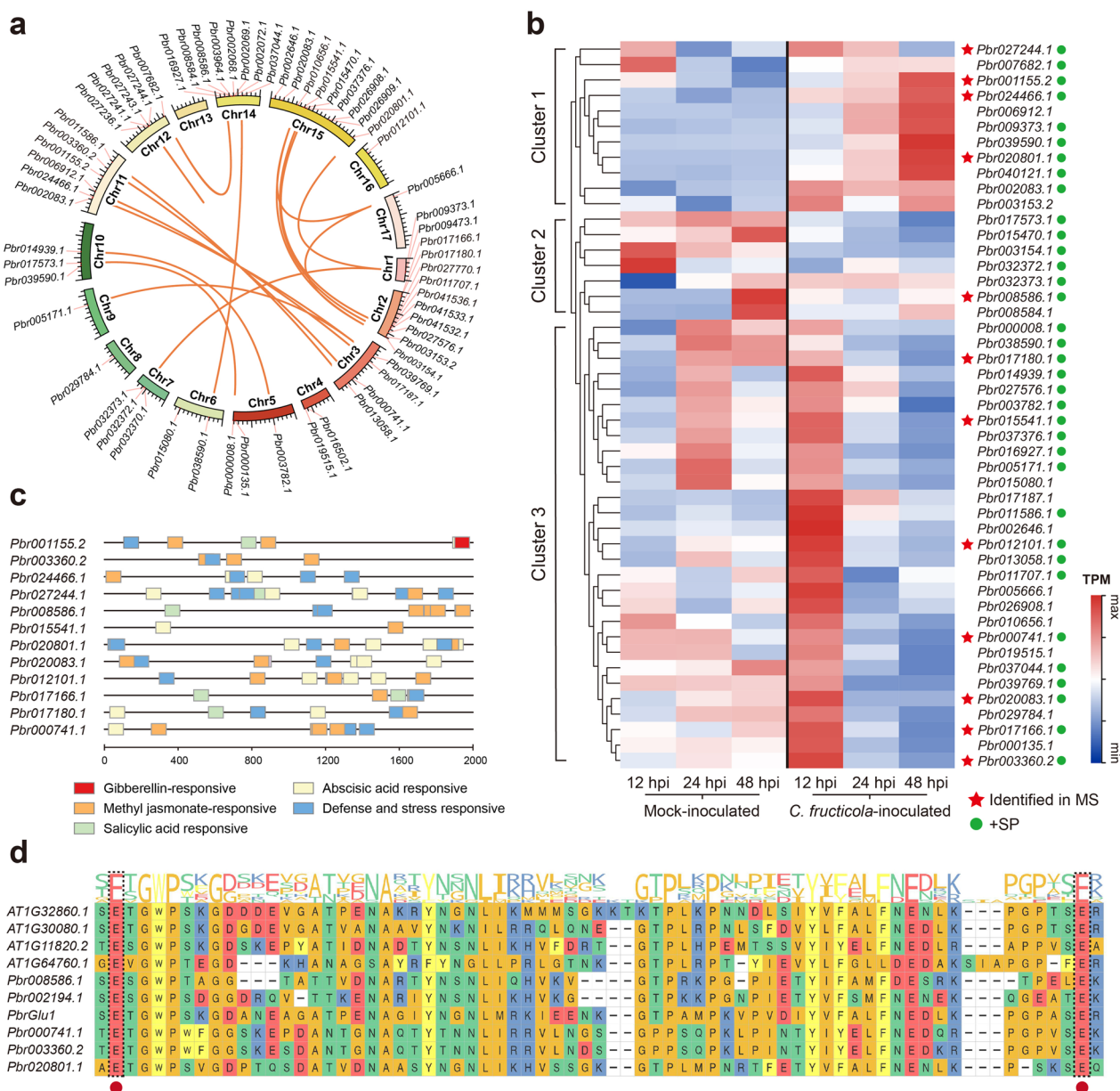
Fig. 7 Evolution, structure, and expression patterns of the GH17 family in *P. bretschneideri*. **a** Gene location and collinearity analysis of GH17 family in *P. bretschneideri*. **b** Expression patterns of GH17 genes during *C. fructicola* infection. The red stars represent proteins identified in the apoplastic fluid, while the circles represent proteins containing signal peptides. **c** The distribution of cis-acting elements in the promoter regions of GH17 genes. **d** The multiple sequence alignment of *P. bretschneideri* GH17 genes with *A. thaliana* GH17 genes, where the predicted enzyme active sites are indicated by boxes

heatmap (Fig. 7b). Cluster 1 contained 11 GH17 genes, most of which exhibited upregulated expression during *C. fructicola* infection and maintained this elevated expression even in the later stages of infection. Cluster 3 encompassed 29 GH17 genes, with majority of these genes showing rapid induction during the early stages of *C. fructicola* infection. However, their expression levels declined significantly as the infection progressed to later

stages. Cluster 2 genes did not display a distinct expression pattern.

To gain insight into the potential mechanisms and transcriptional regulation of the GH17 family in pear plants, the 2000 bp regions upstream of the transcriptional start codons were subjected to analysis using the PlantCare database. This analysis aimed to identify cis-regulatory elements present in these regions. These cis-acting

Han *et al. Phytopathology Research*   (2024) 6:3

Page 10 of 16

regulatory elements were mainly classified into five categories: gibberellin-responsive, abscisic acid responsive, methyl jasmonate-responsive, salicylic acid responsive, and defence and stress responsive (Fig. 7c). The gibberellin-responsive elements are associated with growth and development processes, while abscisic acid-responsive elements are involved in stress responses and abiotic stress signalling. Methyl jasmonate-responsive elements are associated with defence and plant secondary metabolite production, whereas salicylic acid-responsive elements are linked to plant defence against pathogens. Finally, the defence and stress-responsive elements encompass a broader range of stress-related responses. Based on our analysis, we speculate that the GH17 family is involved in various physiological processes and defence responses in pear.

GH17 family members typically possess conserved catalytic active sites, and these active sites play a crucial role in the hydrolysis of glycosidic bonds in various carbohydrates. The beta-1,3-endoglucanase activity of GH17 relies on specific amino acid residues within the active site region. These residues are involved in the hydrolysis of (1−>3)-beta-D-glucosidic linkages in (1−>3)-beta-D-glucans. A multiple sequence alignment was performed using *A. thaliana* and *P. bretschneideri* GH17 domains. The results indicated the presence of two highly conserved glutamic acid residue active sites across all members of the GH17 family (Fig. 7d and Additional file 2: Figure S3a, b). This conservation highlights the critical role of these glutamic acid residues in the catalytic activity of GH17 enzymes and suggests their functional importance across different plant species.

Verification of signal peptide secretion function of *PbrGlu1*

By combining the transcriptomic analysis with the proteomic analysis, a GH17 gene (*PbrGlu1*, *Pbr001155.2*) with higher expression during *C. fructicola* infection was screened through gene family analysis and qRT-PCR (Fig. 7 and Additional file 2: Figure S1). The coding sequence of the N-terminal region of PbrGlu1 (amino acids 1–22) was cloned and inserted into the yeast vector pSUC2, and then all the constructs were transformed into the yeast strain YTK12. The strain containing PsAvr1b was used as the positive control in this assay. All yeast strains were cultured on CMD-W plates and used to select YTK12 harbouring the pSUC2 vector. The strains containing fused *PbrGlu1* and *PsAvr1b* constructs were able to grow on YPRAA medium and enabled the catalysis of 2,3,5-triphenyltetrazolium chloride (TTC) to generate the red coloured product triphenylformazan. In contrast, YTK12 and the strain carrying the pSUC2 vector used as a negative control did not change the colour

of the culture (Fig. 8a). The results confirmed that PbrGlu1 has a secretory signal peptide.

Transient silencing of *PbrGlu1* in pear leaves

To explore the function of *PbrGlu1* after *C. fructicola* infection of pear leaves, we conducted transient silencing of *PbrGlu1* through a virus-induced gene silencing (VIGS) method as previously described (Han et al. 2022). As shown in Fig. 8b and c, the diameter of the diseased area in TRV2-*PbrGlu1* plants after inoculation with *C. fructicola* conidia was more than three-fold greater than that of the CK plants. Although the expression of *PbrGlu1* was upregulated after *C. fructicola* inoculation, the silenced plants still exhibited significantly lower expression compared to the control plants (Fig. 8d). Furthermore, the antioxidant enzyme system served as a crucial indicator for assessing plant disease resistance. We determined the activity of hydrogen peroxide (H_2O_2) and superoxide dismutase (SOD) in the pear leaves. There was no significant difference in hydrogen peroxide content between the CK plants and TRV2-*PbrGlu1* before inoculation. However, after inoculation, the hydrogen peroxide level in TRV2-*PbrGlu1* plants was significantly higher than that in the CK plants (Fig. 8e). The activity of superoxide dismutase in TRV2-*PbrGlu1* plants was also significantly lower than that in the CK plants (Fig. 8f). This evidence uncovered the involvement of the GH17 family gene *PbrGlu1* in the response of pear leaves to *C. fructicola* infection.

Discussion

The apoplast is an essential component of plant physiology and is vital for plant growth, development, and defence against pathogens (Naseem et al. 2017; Wang et al. 2020). Due to the economic importance of *Colletotrichum* spp., they have become the subject of many studies on fungal pathogenicity (Perfect et al. 1999). Research on *Colletotrichum* has unveiled the adoption of a hemibiotrophic lifestyle by multiple phytopathogenic species within the genus (O'Connell et al. 2012; Gan et al. 2013; De Silva et al. 2017). During the early stages of infection, *Colletotrichum* spp. obtained nutrients from living host cells while avoiding cell death or extensive damage (Fig. 1b). This lifestyle enabled us to extract high-quality apoplast fluid during the early stages of infection, avoiding contamination from intracellular components caused by cell death. In this research, we employed the infiltration-centrifugation method as a reliable technique for the successful extraction of apoplast fluid from pear leaves during the early stages of *C. fructicola* infection. By combining the transcriptomic and proteomic analyses, we identified key defence components. A transcriptomic
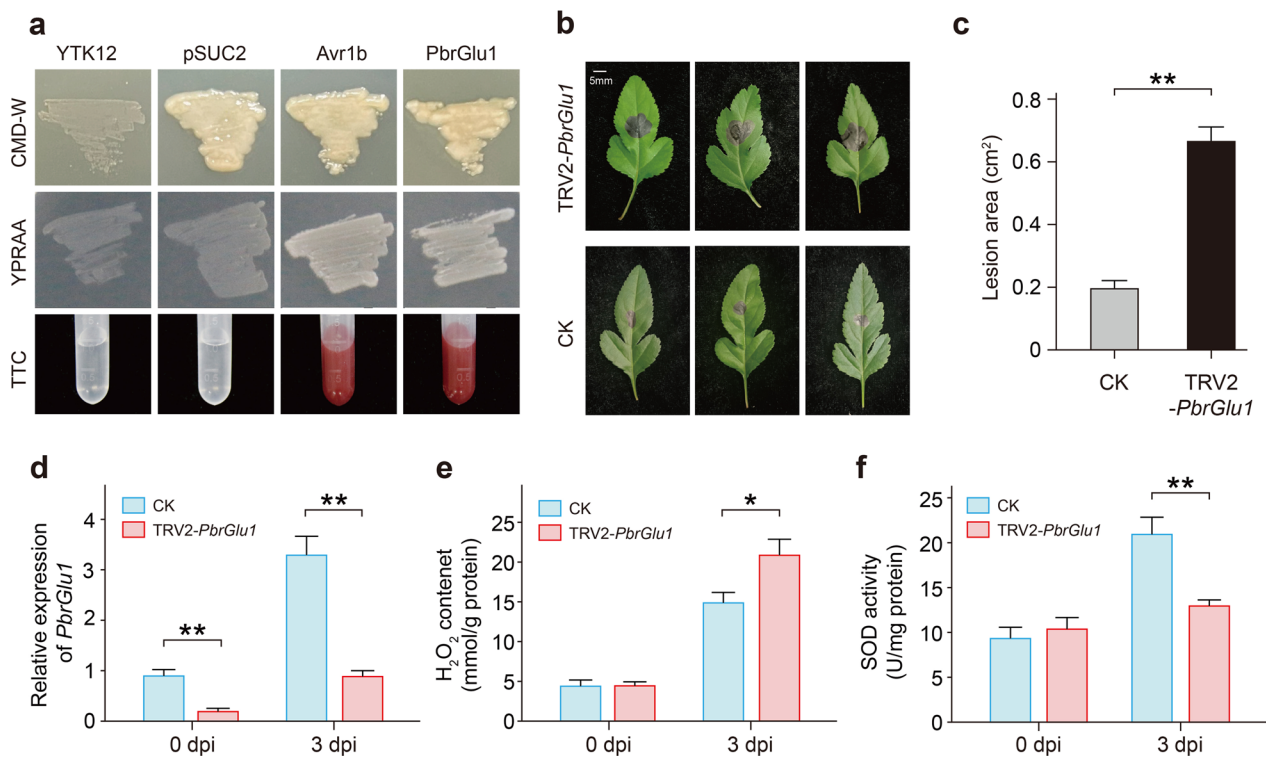
Fig. 8 Functional evaluation of *PbrGlu1* in pear. **a** Functional validation of *PbrGlu1* signal peptide. The strains were cultured on YPDA, CMD-W, or YPRAA medium for two days. Invertase enzymatic activity was assessed by converting 2,3,5-triphenyl tetrazolium chloride (TTC) into insoluble red-colored 1,3,5-triphenyl formazan. **b** Phenotype of CK and TRV2-*PbrGlu1* during *C. fructicola* infection of pear leaves at 3 dpi. **c** Disease spot diameter in TRV2-*PbrGlu1* leaves and CK leaves. **d** Expression patterns of CK and TRV2-*PbrGlu1* before and after inoculation. **e** Changes in hydrogen peroxide content. **f** Changes in SOD activity. * indicated significant differences, * $p < 0.05$, ** $p < 0.01$

analysis enabled us to identify and quantify changes in gene expression, providing insights into the activation of defence pathways, metabolic adjustments, and signalling cascades taking place in the apoplast.

To date, research on the interaction between pear and *C. fructicola* remains limited. By employing RNA-seq technology, we unveiled extensive changes at the RNA level in pear upon infection with anthracnose disease (Fig. 2). Compared to the mock-inoculated group, induction of defence-related genes were observed in the early stages of infection, and there were temporal expression differences at different time points (Fig. 2b, c). These findings are similar to that in the pear response to *Botryosphaeria dothidea* infection (Wang et al. 2022). The GO analysis revealed that the DEGs were mainly involved in various hydrolase activities, kinase activities, and defence responses against fungi (Fig. 2d). The highest ranked terms in the GO cellular component included vacuole, apoplast, cell wall, extracellular region, and intrinsic component of membrane. Cell walls provide structural support and protection (Bacete et al. 2018), while vacuoles play crucial roles in storage, detoxification, and osmotic regulation (Jiang et al. 2021). The extracellular regions

serve as sites for intercellular communication and signalling (Tabassum et al. 2022). These findings substantiate the pivotal role of the apoplast as a crucial site for pear resistance against anthracnose disease.

More than 50% of the apoplastic proteins contained signal peptides, the proportion significantly higher than that found in the total pear proteome. Although previous studies have found that approximately 50% of secreted proteins in plants lack a well-defined signal peptide (Agrawal et al. 2010), our results indicated that the classical secretory pathway remains the major pathway for protein secretion in pears. Most SP-containing proteins secreted into the apoplast are hydrolytic enzymes. These proteins, including glycosidases, proteases, and esterases, play a significant role in plant defence and plant-pathogen interactions (Fig. 4). Glycosidases are involved in carbohydrate metabolism and the breakdown of cell wall components, contributing to cell wall remodelling and defence against pathogens (Gomez et al. 2002). Proteases are responsible for the degradation and processing of proteins, which can potentially influence the activation of defence-related proteins or be utilized to attack effector proteins secreted by pathogens (Wang

et al. 2019, 2020). Esterases, on the other hand, participate in the hydrolysis of ester bonds and may be involved in lipid metabolism and signalling pathways associated with plant defence (Shen et al. 2022; Xiao et al. 2022). We analysed the expression levels of apoplastic hydrolases during *C. fructicola* infection, and majority of the genes showed an upregulation trend during the early stages (Fig. 5a, b). In the later stages of infection (48 hpi), there was a notable increase in the number of downregulated genes. It indicates that the apoplastic defence response in plants is highly rapid. However, the exact reason for this downregulation in the later stages, whether it is due to plant intrinsic factors or regulation by pathogen effectors, remains unknown. Previous studies have reported that pathogen effectors can target key signalling hubs in plants, such as the TAP (transcriptional activator protein) and JAZ (jasmonate ZIM-domain) transcription factors (Gonzalez-Fuente et al. 2020; Ceulemans et al. 2021). This mechanism may also exist in pear-*C. fructicola* interaction. Furthermore, through coexpression network analysis, we observed extensive coexpression among the hydrolases, implying potential regulation by shared transcription factors or common regulatory mechanisms.

The GH17 family was found to represent the most abundant group of glycosidases identified in pear leaves in this study, comprising 17 distinct members. Previous studies have reported that GH17 plays an important role in the response to environmental stresses for plant adaptation and the grape GH17 family genes *VvEGase1* and *VvEGase3* can interfere with cell wall synthesis and inhibit spore germination of *Plasmopara viticola in vitro* (Mestre et al. 2017). Overexpression of the GH17 family gene G2 in *A. thaliana* enhanced resistance to dehydration and NaCl stress (Xu et al. 2012). Moreover, several studies have revealed that alterations in reactive oxygen species (ROS) levels provide valuable insights into the pathogen response (Wang et al. 2022). Therefore, we silenced *PbrGlu1* by VIGS and found that *C. fructicola* infection increased the expression of TRV-*PbrGlu1* in pear and that the defective pear seedlings showed more severe symptoms and higher H_2O_2 contents after inoculation, revealing that *C. fructicola* infection increased the sensitivity of the TRV-*PbrGlu1* lines, consistent with previous studies.

Conclusions

This study utilized centrifugation to extract apoplast fluid and applied proteomics and transcriptomics analysis to investigate the molecular responses of pear leaves during pathogen recognition and defence mechanisms. The findings included the first description of apoplast fluid components, their functions, and expression patterns in pear leaves. Notably, a substantial induction of hydrolytic

enzymes was observed during the early stages of infection, displaying a clear coexpression pattern. In addition, we identified a GH17 family gene, *PbrGlu1*, through expression pattern screening. Transient silencing of *PbrGlu1* reduced the resistance of pear against the pathogen, indicating that *PbrGlu1* played a significant role in pear disease resistance. Based on these research findings, we have gained a comprehensive understanding of the apoplastic defence against *C. fructicola* infection in pear leaves. In summary, exploring the apoplastic battlefield to identify these pathogen-responsive hydrolases is an exciting new approach to discover novel components of plant cell wall immunity.

Methods

Plants, fungal strains, and treatments

The 'Cuiguan' pear tree originated from the Jiangpu experimental orchard of Nanjing Agricultural University. The mature leaves were collected from the new shoots of the current year, 20 days after they emerged, from late May to early June. Samples were selected with uniform size, free from diseases and pests, and without pesticide spraying, to be used as experimental materials. The collected leaves underwent a sterilization process using 0.1% sodium hypochlorite solution for a duration of 10 min. Subsequently, the leaves were thoroughly rinsed with distilled water 3–4 times to eliminate any remaining traces of sodium hypochlorite. These leaves were used for apoplast fluid isolation. The pear seedlings used for agroinfiltration were grown from seeds and were 35 days old at the time of the experiment. These seedlings were cultivated in a greenhouse under a 16-h light and 8-h dark photoperiod, with 75% relative humidity, and at a temperature of 25°C.

The *C. fructicola* fungal strain NC40 used in this study were routinely cultured on potato dextrose agar (PDA) at 28°C as described previously (Li et al. 2022). To obtain fresh conidia, a 5-mm-diameter mycelial plug was placed in a 100-mL flask containing 50 mL of sterilized potato dextrose broth (PDB). The flasks were shaken at 180 rpm at 28°C for 4 days. The concentration of the conidial suspension was determined using a hemocytometer. Conidia were collected, suspended in sterilised water, diluted to a concentration of 1×10^4 conidia per mL.

The field-collected leaves used for apoplast fluid isolation were conducted using soaking inoculation with a conidial suspension. Fresh leaves were fully immersed in a conidial suspension for half an hour with gentle agitation, while the control group was mock-inoculated with pure water. The inoculated leaves were cultured at a temperature of 25°C and a relative humidity of 80%. Samples were collected at 12 hpi, 24 hpi, and 48 hpi. Five leaf samples were collected at each time point. For

RNA-seq analysis, the samples were immediately flash-frozen in liquid nitrogen and stored at -80°C. Samples collected for apoplast fluid extraction were used in experiments without delay. This experiment was repeated three times.

RNA isolation, identification, and library construction

RNA extraction and sequencing were performed by Novogene Corporation (Nanjing, China). Total RNA was extracted using the Plant RNA Isolation Kit (Macrogen). The purity of RNA was assessed using the NanoPhotometer spectrophotometer (IMPLEN, CA, United States), and the concentration was measured using the Qubit RNA Assay Kit by the Qubit 2.0 Fluorometer (Life Technologies, CA, United States). RNA integrity was evaluated using the RNA Nano 6000 Assay Kit on the Bioanalyzer 2100 system (Agilent Technologies, CA, United States). For RNA sample preparations, 3 mg of RNA per sample was used as input material. NEBNext Ultra RNA Library Prep Kit for Illumina (NEB, United States) was utilized to generate sequencing libraries. The libraries were sequenced on an Illumina Hiseq platform, producing 125 bp/150 bp paired-end reads.

The raw data (raw reads) in fastq format was initially processed using in-house perl scripts to obtain clean reads. This process involved removing reads containing adapters, reads containing poly-N sequences, and low-quality reads from the raw data. Quality metrics such as Q30, Q20, and GC content were calculated for each sample, and subsequent analyses were performed based on the clean data. The clean reads were aligned to the genome of the Chinese white pear (cv. "Dangshansuli") using HISAT2 (Kim et al. 2015). The read counts for each sample were obtained using FeatureCounts (Liao et al. 2014). Finally, the read counts were normalized to tags per million (TPM) using TBtools (Chen et al. 2020).

Apoplast fluid isolation

The apoplast fluid was extracted from the infected leaves at 12 hpi. In brief, a vacuum was applied using a pump and then released to facilitate water intake. Subsequently, the leaves were rolled into a 50 mL syringe without a plunger, placed in a 50 mL tube, and centrifuged at 1500 *g* for 45 min at 4°C, with a slow acceleration and deceleration of the rotor. The apoplast fluid was collected from the bottom of the 50 mL tube and further filtered through 0.25-mm membrane column (Merck Millipore, St. Louis, MO, USA).

Identification of apoplastic proteins through LC–MS/MS

Identification of apoplast proteins was performed using liquid chromatography/mass spectrometry (LC-MS/MS), following the previously described method (Sabehi et al. 2012). Briefly, ancestral S-TIM4 particles were purified using CsCl and then digested with modified trypsin (Promega). The digested and purified peptides were subjected to LC-MS/MS analysis using a mass spectrometer (Q-Exactive HF X, Thermo Scientific). Data analysis was conducted using Mascot v2.3.02 software, searching against the *P. bretschneideri* genome.

Differential expression and gene enrichment analysis

The read counts were utilized for conducting differential gene expression analysis using the DESeq2 package (v1.30.1). Genes with $|\log_2(\text{fold change})| \geq 1$ and adjusted *P*-value < 0.01 were classified as DEGs. Gene Ontology (GO) and pathway annotation and enrichment analyses were based on the eggNOG (http://eggnog-mapper.embl.de/) (Huerta-Cepas et al. 2019), Gene Ontology Database (http://www.geneontology.org/), and KEGG pathway database (http://www.genome.jp/kegg/).

Coexpression network analysis of apoplast hydrolases

RNA-seq data were utilized to investigate the expression patterns of apoplast hydrolase genes. The expression similarity between pairs of genes was measured using Pearson's correlation coefficient (PCC). The PCC values were subsequently filtered with a threshold set at > 0.8. Visualization of the data was carried out using Cytoscape software (Shannon et al. 2003).

Identification of GH17 genes in pear

The genome sequence of *P. bretschneideri* was obtained from the pear genome project (http://peargenome.njau.edu.cn/) (Wu et al. 2013). HMM profiles for the GH17 family (PF00332) were downloaded from Pfam (http://pfam.xfam.org). Subsequently, an HMM search was conducted against the *P. bretschneideri* protein databases using HMMER3. To eliminate redundant and incomplete sequences, overlapping genes were excluded, the CDD tool (https://www.ncbi.nlm.nih.gov/cdd) was employed to ensure the completeness of the conserved domains.

Chromosome location and synteny analysis

The chromosome location information of *P. bretschneideri* was extracted from their respective genome annotations. Synteny analysis among these genomes

was conducted using a methodology similar to PGDD (http://chibba.agtec.uga.edu/duplication/) (Lee et al. 2013). Initially, BLASTp was employed to identify homologous gene pairs across the multiple genomes. Subsequently, collinearity analyses were performed using MCScanX software, and the results were visualized using TBtools (Wang et al. 2012; Chen et al. 2020).

Analysis of cis-acting elements in the promoter regions of GH17 genes in pear

In this study, the promoter regions were defined as 2000 bp upstream from the transcription start site of each gene. The analysis of cis-acting elements within these promoter regions was conducted using PlantCARE (http://bioinformatics.psb.ugent.be/webtools/plantcare).

Functional verification of *PbrGlu1* signal peptide

The predicted N-terminal 22-amino acid signal peptide (SP) sequence of *PbrGlu1* was fused in-frame with the invertase gene in the pSUC2 vector. The pSUC2 vector contains the sucrose invertase gene SUC2 without the initiation ATG codon and was subsequently transformed into yeast strain YTK12. EcoRI and XhoI restriction enzymes were utilized to insert the SP sequences into the pSUC2 vector. The transformant strains were then screened on YPDA, CMD-W, and selective YPRAA plates. YTK12 strains harboring the empty pSUC vector or pSUC2-Avr1bSP were employed as negative and positive controls, respectively. Enzymatic activity was assessed by reducing 2,3,5-triphenyl tetrazolium chloride to form red 1,3,5-triphenyl formazan.

Transient silencing of *PbrGlu1* in pear leaves

Virus-induced gene silencing (VIGS) was performed following previously established methods (Han et al. 2022). The 237 bp open reading frame (ORF) of PbrGlu1 was inserted into the EcoR I and BamH I sites of the tobacco rattle virus-based vector 2 (TRV2) to create the *PbrGlu1*-VIGS construct. The primers used are listed in Additional file 1: Table S4. *A. tumefaciens* strain GV3101 was transformed with the vectors pTRV1, pTRV2, and *PbrGlu1*-pTRV2 using heat shock. The bacterial cells ($OD_{600} = 1.0$) containing pTRV1 were mixed with *PbrGlu1*-pTRV2 or pTRV2 in a 1:1 volume ratio in 2-(morpholino) ethane-sulfonic acid (MES) buffer (10 mM $MgCl_2$, 200 mM acetosyringone, and 10 mM MES, pH 5.6) and incubated in the dark with gentle shaking for 4 h at room temperature. Then, the re-suspended *A. tumefaciens* was injected into the abaxial side of the leaves using a 1-mL syringe (without needles). pTRV1 and pTRV2 injections were used as the control (CK) group. After two weeks, upper leaves were collected from each plant for qRT-PCR analysis.

The PbrGlu1 expression in VIGS plants was significantly reduced. Finally, upper leaves were collected, and each leaf was inoculated with a *C. fructicola* mycelial cake (with a diameter of 5 mm) and incubated in the dark at 26℃. The contents of H_2O_2 and SOD were detected according to the manufacturer's instructions (Comin, Suzhou, China). The same experiment was repeated three times.

Abbreviations

AM	Arbuscular mycorrhizal
APs	Aspartyl proteases
CEHs	Carboxylic-ester hydrolases
CPs	Cyseine proteases
DEGs	Differentially expressed genes
EHM	Extrahaustorial membrane
EIHM	Extrainvasive hyphae membrane
GHs	Glycoside hydrolases
HPI	Hours post-inoculation
JAZ	Jasmonate ZIM-domain
PAM	Periarbuscular membrane
PCC	Pearson's correlation coefficient
PDA	Potato dextrose agar
PDB	Potato dextrose broth
PDHs	Phosphoric-diester hydrolases
RNA-seq	RNA sequencing
PR	Pathogenesis-related
ROS	Reactive oxygen species
SEPs	Serine proteases
SP	Signal peptide
TAP	Transcriptional activator protein

Supplementary Information

The online version contains supplementary material available at https://doi.org/10.1186/s42483-023-00220-x.

Additional file 1: Table S1. The RNA-seq read counts and mapping rates of different samples from pear leaves after *C. fructicola* inoculation and mock inoculation. **Table S2**. List the detailed information of pear apoplast proteins. **Table S3**. The members of GH17 gene family in Chinese White pear genome. **Table S4**. Primers were used in this study.

Additional file 2: Figure S1. The relative expression levels of several apoplast proteins genes in *C. fructicola* infected plants and healthy plants. Bar values represent the means SEM of three biological replicates with three technical replicates. * indicate significant differences, * $p<0.05$, ** $p<0.01$. **Figure S2**. Phylogeny and conserved motifs of GH17 gene family genes in pear. The conserved motifs were analyzed by the MEME tool (http://memesuite.org/) using the default settings. **Figure S3**. Predicted protein structures of PbrGlu1 and AT1G32860.1. **a** The predicted Pfam domain of PbrGlu1 and AT1G32860.1. **b** Schematic representation of PbrGlu1 and AT1G32860.1 model based on the predicted protein structure from UniProt (https://www.uniprot.org/).

Han *et al. Phytopathology Research*   (2024) 6:3

Page 15 of 16

Declarations

Ethics approval and consent to participate
Not applicable.

Consent for publication
Not applicable.

Competing interests
The authors declare that they have no competing interests.

References

Agrawal GK, Jwa NS, Lebrun MH, Job D, Rakwal R. Plant secretome: unlocking secrets of the secreted proteins. Proteomics. 2010;10(4):799–827. https://doi.org/10.1002/pmic.200900514.

Bacete L, Melida H, Miedes E, Molina A. Plant cell wall-mediated immunity: cell wall changes trigger disease resistance responses. Plant J. 2018;93(4):614–36. https://doi.org/10.1111/tpj.13807.

Bai Y, Muller DB, Srinivas G, Garrido-Oter R, Potthoff E, Rott M, et al. Functional overlap of the Arabidopsis leaf and root microbiota. Nature. 2015;528(7582):364–9. https://doi.org/10.1038/nature16192.

Bhadouria J, Giri J. Purple acid phosphatases: roles in phosphate utilization and new emerging functions. Plant Cell Rep. 2022;41:33–51. https://doi.org/10.1007/s00299-021-02773-7.

Buscaill P, Chandrasekar B, Sanguankiattichai N, Kourelis J, Kaschani F, Thomas EL, et al. Glycosidase and glycan polymorphism control hydrolytic release of immunogenic flagellin peptides. Science. 2019;364(6436):145. https://doi.org/10.1126/science.aav0748.

Cao M, Zhang Z, Tian H, Yu W, Zhao X, Yang W, et al. The histone deacetylase Cfhos2 is a key epigenetic factor regulating appressorium development and pathogenesis in apple Glomerella leaf spot fungus *Colletotrichum fructicola*. Phytopathol Res. 2022;38(1):219–26. https://doi.org/10.1186/s42483-022-00144-y.

Ceulemans E, Ibrahim HMM, De Coninck B, Goossens A. Pathogen effectors: exploiting the promiscuity of plant signaling hubs. Trends Plant Sci. 2021;26(8):780–95. https://doi.org/10.1016/j.tplants.2021.01.005.

Chen C, Chen H, Zhang Y, Thomas HR, Frank MH, He Y, et al. TBtools: an integrative toolkit developed for interactive analyses of big biological data. Mol Plant. 2020;13(8):1194–202. https://doi.org/10.1016/j.molp.2020.06.009.

Christensen AB, Cho BH, Næsby M, Gregersen PL, Brandt J, Madriz-Ordeñana K, et al. The molecular characterization of two barley proteins establishes the novel PR-17 family of pathogenesis-related proteins. Mol Plant Pathol. 2002;3(3):135–44. https://doi.org/10.1046/j.1364-3703.2002.00105.

De Silva DD, Crous PW, Ades PK, Hyde KD, Taylor PWJ. Life styles of *Colletotrichum* species and implications for plant biosecurity. Fungal Biol Rev. 2017;31(3):155–68. https://doi.org/10.1016/j.fbr.2017.05.001.

Dora S, Terrett OM, Sanchez-Rodriguez C. Plant-microbe interactions in the apoplast: communication at the plant cell wall. Plant Cell. 2022;34(5):1532–50. https://doi.org/10.1093/plcell/koac040.

Fu M, Crous PW, Bai Q, Zhang PF, Xiang J, Guo YS, et al. *Colletotrichum* species associated with anthracnose of *Pyrus* spp. in China. Persoonia. 2019;42:1–35. https://doi.org/10.3767/persoonia.2019.42.01.

Gan P, Ikeda K, Irieda H, Narusaka M, O'Connell RJ, Narusaka Y, et al. Comparative genomic and transcriptomic analyses reveal the hemibiotrophic stage shift of *Colletotrichum* fungi. New Phytol. 2013;197(4):1236–49. https://doi.org/10.1111/nph.12085.

Gentzel I, Giese L, Zhao W, Alonso AP, Mackey D. A simple method for measuring apoplast hydration and collecting apoplast contents. Plant Physiol. 2019;179(4):1265–72. https://doi.org/10.1104/pp.18.01076.

Giraldo MC, Valent B. Filamentous plant pathogen effectors in action. Nat Rev Microbiol. 2013;11(11):800–14. https://doi.org/10.1038/nrmicro3119.

Gomez L, Allona I, Casado R, Aragoncillo C. Seed chitinases. Seed Sci Res. 2002;12(4):217–30. https://doi.org/10.1079/SSR2002113.

Gonzalez-Fuente M, Carrere S, Monachello D, Marsella BG, Cazale AC, Zischek C, et al. EffectorK, a comprehensive resource to mine for Ralstonia, Xanthomonas, and other published effector interactors in the *Arabidopsis* proteome. Mol Plant Pathol. 2020;21(10):1257–70. https://doi.org/10.1111/mpp.12965.

Han C, Dong H, Qiao Q, Dai Y, Huang X, Zhang S. Comparative genomic analysis of N^6-methyladenosine regulators in nine rosaceae species and functional characterization in response to drought stress in pear. Horticol Plant J. 2022;9(4):693–704. https://doi.org/10.1016/j.hpj.2022.09.008.

Hong JK, Hwang BK. Induction by pathogen, salt and drought of a basic class II chitinase mRNA and its in situ localization in pepper (*Capsicum annuum*). Physiol Plant. 2002;114(4):549–58. https://doi.org/10.1034/j.1399-3054.2002.1140407.x.

Huerta-Cepas J, Szklarczyk D, Heller D, Hernandez-Plaza A, Forslund SK, Cook H, et al. eggNOG 5.0: a hierarchical, functionally and phylogenetically annotated orthology resource based on 5090 organisms and 2502 viruses. Nucleic Acids Res. 2019;47(D1):D309–14. https://doi.org/10.1093/nar/gky1085.

Ivanov S, Austin J, Berg RH, Harrison MJ. Extensive membrane systems at the host-arbuscular mycorrhizal fungus interface. Nat Plants. 2019;5(2):194–203. https://doi.org/10.1038/s41477-019-0364-5.

Jiang J, Zhai H, Li H, Wang Z, Chen Y, Hong N, et al. Identification and characterization of *Colletotrichum fructicola* causing black spots on young fruits related to bitter rot of pear (*Pyrus bretschneideri Rehd.*) in China. Crop Prot. 2014;58:41–8. https://doi.org/10.1016/j.cropro.2014.01.003.

Jiang YT, Yang LH, Ferjani A, Lin WH. Multiple functions of the vacuole in plant growth and fruit quality. Mol Hortic. 2021;1(1):1–13. https://doi.org/10.1186/s43897-021-00008-7.

Kankanala P, Czymmek K, Valent B. Roles for rice membrane dynamics and plasmodesmata during biotrophic invasion by the blast fungus. Plant Cell. 2007;19(2):706–24. https://doi.org/10.1105/tpc.106.046300.

Kim D, Langmead B, Salzberg SL. HISAT: a fast spliced aligner with low memory requirements. Nat Methods. 2015;12:357–60. https://doi.org/10.1038/nmeth.3317.

Kwaaitaal M, Nielsen ME, Bohlenius H, Thordal-Christensen H. The plant membrane surrounding powdery mildew haustoria shares properties with the endoplasmic reticulum membrane. J Exp Bot. 2017;68(21–22):5731–43. https://doi.org/10.1093/jxb/erx403.

Lee C, Verma R, Byun S, Jeun EJ, Kim GC, Lee S, et al. Structural specificities of cell surface beta-glucan polysaccharides determine commensal yeast mediated immuno-modulatory activities. Nat Commun. 2021;12(1):3611. https://doi.org/10.1038/s41467-021-23929-9.

Lee TH, Tang H, Wang X, Paterson AH. PGDD: a database of gene and genome duplication in plants. Nucleic Acids Res. 2013;41(D1):D1152–8. https://doi.org/10.1093/nar/gks1104.

Li C, Sun W, Cao S, Hou R, Li X, Ming L, et al. The CfMK1 gene regulates reproduction, appressorium formation, and pathogenesis in a pear anthracnose-causing fungus. J Fungi. 2022;8(1):77. https://doi.org/10.3390/jof8010077.

Li HN, Jiang JJ, Hong N, Wang GP, Xu WX. First report of Colletotrichum fructicola causing bitter rot of pear (*Pyrus bretschneideri*) in China. Plant Dis. 2013;97(7):1000. https://doi.org/10.1094/PDIS-01-13-0084-PDN.

Liao Y, Smyth GK, Shi W. Feature counts: an efficient general purpose program for assigning sequence reads to genomic features. Bioinformatics. 2014;30(7):923–30. https://doi.org/10.1093/bioinformatics/btt656.

Lo Presti L, Lanver D, Schweizer G, Tanaka S, Liang L, Tollot M, et al. Fungal effectors and plant susceptibility. Annu Rev Plant Biol. 2015;66:513–45. https://doi.org/10.1146/annurev-arplant-043014-114623.

Lohaus G, Pennewiss K, Sattelmacher B, Hussmann M, Hermann MK. Is the infiltration-centrifugation technique appropriate for the isolation of apoplastic fluid? A critical evaluation with different plant species. Physiol Plant. 2001;111(4):457–65. https://doi.org/10.1034/j.1399-3054.2001.1110405.x.

Lopez-Casado G, Urbanowicz BR, Damasceno CM, Rose JK. Plant glycosyl hydrolases and biofuels: a natural marriage. Curr Opin Plant Biol. 2008;11(3):329–37. https://doi.org/10.1016/j.pbi.2008.02.010.

Ma Z, Zhu L, Song T, Wang Y, Zhang Q, Xia Y, et al. A paralogous decoy protects *Phytophthora sojae* apoplastic effector PsXEG1 from a host inhibitor. Science. 2017;355(6326):710–4. https://doi.org/10.1126/science.aai7919.

Maxwell TL, Canarini A, Bogdanovic I, Böckle T, Martin V, Noll L, et al. Contrasting drivers of belowground nitrogen cycling in a montane grassland exposed to a multifactorial global change experiment with elevated CO_2, warming, and drought. Global Change Biol. 2022;28(7):2425–41. https://doi.org/10.1111/gcb.16035.

Mestre P, Arista G, Piron MC, Rustenholz C, Ritzenthaler C, Merdinoglu D, et al. Identification of a *Vitis vinifera* endo-beta-1,3-glucanase with antimicrobial activity against Plasmopara viticola. Mol Plant Pathol. 2017;18(5):708–19. https://doi.org/10.1111/mpp.12431.

Kidwai M, Ahmad IZ, Chakrabarty D. Class III peroxidase: an indispensable enzyme for biotic/abiotic stress tolerance and a potent candidate for crop improvement. Plant Cell Rep. 2020;39(11):1381–93. https://doi.org/10.1007/s00299-020-02588-y.

Naseem M, Kunz M, Dandekar T. Plant-pathogen maneuvering over apoplastic sugars. Trends Plant Sci. 2017;22(9):740–3. https://doi.org/10.1016/j.tplants.2017.07.001.

O'Connell RJ, Thon MR, Hacquard S, Amyotte SG, Kleemann J, Torres MF, et al. Lifestyle transitions in plant pathogenic *Colletotrichum* fungi deciphered by genome and transcriptome analyses. Nat Genet. 2012;44(9):1060–5. https://doi.org/10.1038/ng.2372.

Perfect SE, Hughes HB, O'Connell RJ, Green JR. *Colletotrichum*: a model genus for studies on pathology and fungal–plant interactions. Fungal Genet Biol. 1999;27(2–3):186–98. https://doi.org/10.1006/fgbi.1999.1143.

Philippe F, Pelloux J, Rayon C. Plant pectin acetylesterase structure and function: new insights from bioinformatic analysis. BMC Genom. 2017;18:456. https://doi.org/10.1186/s12864-017-3833-0.

Qin Q, Bergmann CW, Rose JK, Saladie M, Kolli VK, Albersheim P, et al. Characterization of a tomato protein that inhibits a xyloglucan-specific endoglucanase. Plant J. 2003;34(3):327–38. https://doi.org/10.1046/j.1365-313X.2003.01726.x.

Sabehi G, Shaulov L, Silver DH, Yanai I, Harel A, Lindell D. A novel lineage of myoviruses infecting cyanobacteria is widespread in the oceans. Proc Natl Acad Sci. 2012;109(6):2037–42. https://doi.org/10.1073/pnas.1115467109.

Sattelmacher B. The apoplast and its significance for plant mineral nutrition. New Phytol. 2000;149:167–92. https://doi.org/10.1046/j.1469-8137.2001.00034.x.

Shannon P, Markiel A, Ozier O, Baliga NS, Wang JT, Ramage D, et al. Cytoscape: a software environment for integrated models of biomolecular interaction networks. Genome Res. 2003;13(11):2498–504. https://doi.org/10.1101/gr.1239303.

Shen G, Sun W, Chen Z, Shi L, Hong J, Shi J. Plant GDSL esterases/lipases: evolutionary, physiological and molecular functions in plant development. Plants. 2022;11(4):468. https://doi.org/10.3390/plants11040468.

Sueldo DJ, Godson A, Kaschani F, Krahn D, Kessenbrock T, Buscaill P, et al. Activity-based proteomics uncovers suppressed hydrolases and a neo-functionalised antibacterial enzyme at the plant-pathogen interface. New Phytol. 2023. https://doi.org/10.1111/nph.18857.

Tabassum N, Blilou I. Cell-to-cell communication during plant-pathogen interaction. Mol Plant Microbe Interact. 2022;35(2):98–108. https://doi.org/10.1094/MPMI-09-21-0221-CR.

van Loon LC, Rep M, Pieterse CM. Significance of inducible defense-related proteins in infected plants. Annu Rev Phytopathol. 2006;44:135–62. https://doi.org/10.1146/annurev.phyto.44.070505.143425.

Wang S, Xing R, Wang Y, Shu H, Fu S, Huang J, et al. Cleavage of a pathogen apoplastic protein by plant subtilases activates host immunity. New Phytol. 2021;229(6):3424–39. https://doi.org/10.1111/nph.17120.

Wang Y, Sun X, Zhang Z, Pan B, Xu W, Zhang S. Revealing the early response of pear (*Pyrus bretschneideri Rehd*) leaves during Botryosphaeria dothideainfection by transcriptome analysis. Plant Sci. 2022;315:111146. https://doi.org/10.1016/j.plantsci.2021.111146.

Wang Y, Garrido-Oter R, Wu J, Winkelmüller TM, Agler M, Colby T, et al. Site-specific cleavage of bacterial MucD by secreted proteases mediates antibacterial resistance in Arabidopsis. Nat Commun. 2019;10(1):2853. https://doi.org/10.1038/s41467-019-10793-x.

Wang Y, Tang H, DeBarry JD, Tan X, Li J, Wang X, et al. MCScanX: a toolkit for detection and evolutionary analysis of gene synteny and collinearity. Nucleic Acids Res. 2012;40(7):e49. https://doi.org/10.1093/nar/gkr1293.

Wang Y, Wang Y, Wang Y. Apoplastic proteases: powerful weapons against pathogen infection in plants. Plant Commun. 2020;1(4):100085. https://doi.org/10.1016/j.xplc.2020.100085.

Witzel K, Shahzad M, Matros A, Mock HP, Mühling KH. Comparative evaluation of extraction methods for apoplastic proteins from maize leaves. Plant Methods. 2011;7:1–11. https://doi.org/10.1186/1746-4811-7-48.

Wei W, Riley NM, Yang AC, Kim JT, Terrell SM, Li VL, Garcia-Contreras M, Bertozzi CR, Long JZ. Cell type-selective secretome profiling in vivo. Nat Chem Biol. 2021;17(3):326–34. https://doi.org/10.1038/s41589-020-00698-y.

Wu J, Wang Z, Shi Z, Zhang S, Ming R, Zhu S, et al. The genome of the pear (*Pyrus bretschneideri Rehd*.). Genome Res. 2013;23(2):396–408. https://doi.org/10.1101/gr.144311.112.

Xiao R, Zou Y, Guo X, Li H, Lu H. Fatty acid desaturases (FADs) modulate multiple lipid metabolism pathways to improve plant resistance. Mol Bio Rep. 2022;49(10):9997–10011. https://doi.org/10.1007/s11033-022-07568-x.

Xu ZY, Lee KH, Dong T, Jeong JC, Jin JB, Kanno Y, et al. A vacuolar beta-glucosidase homolog that possesses glucose-conjugated abscisic acid hydrolyzing activity plays an important role in osmotic stress responses in Arabidopsis. Plant Cell. 2012;24(5):2184–99. https://doi.org/10.1105/tpc.112.095935.

Yoshida K, Kaothien P, Matsui T, Kawaoka A, Shinmyo A. Molecular biology and application of plant peroxidase genes. Appl Microbiol Biotechnol. 2003;60(6):665–70. https://doi.org/10.1007/s00253-002-1157-7.

Zribi I, Ghorbel M, Brini F. Pathogenesis related proteins (PRs): from cellular mechanisms to plant defense. Curr Protein Pept Sci. 2021;22(5):396–412. https://doi.org/10.2174/1389203721999201231212736.

Publisher's Note